

Indian Journal of Chemistry
Vol. 58A, August 2019, pp. 867-873

CeO₂ nanowires inserted into reduced graphene oxide as active electrocatalyst for oxygen reduction reaction

Yabo Sun^b, Yuanyuan Chu^{a,b,c,*}, Xiaoming Xia^b, Haitao Wang^b, Xiaoyao Tan^{a,b,*}, Zhao Dai^b & Liang Wang^a

^aState Key Laboratory of Separation Membranes and Membrane Processes, Tianjin Polytechnic University,
No.399 Binshui West Road, Tianjin 300387, China

^bSchool of Environmental and Chemical Engineering, Tianjin Polytechnic University, No.399 Binshui West Road, Tianjin 300387, China

^cTianjin Key Laboratory of Advanced Fibers and Energy Storage, Tianjin Polytechnic University, No.399 Binshui West Road,
Tianjin 300387, China

Email: chuyuan1982@163.com

Received 20 August 2018; revised and accepted 24 June 2019

Fabrication of an interconnected and conductive nano-architecture has been a prospective strategy to design a high-performance and low cost electrocatalyst for oxygen reduction reaction (ORR). Herein, a novel nano-architecture assembled by graphene nanosheets and CeO₂ nanowires (NWs) with a hierarchical structure has been developed by a facile hydrothermal process using ethanol/water as solvents without any organic additives. In this framework, graphene oxide (GO) has been reduced to graphene and chemical bonding formed between the GO and CeO₂ NWs in a hydrothermal process. The imbedded CeO₂ NWs has been prevent the restacking of the graphene sheets and improved the electrical conductivity of the hybrid catalyst. The effect of different ratios of GO to CeO₂ NWs in the hybrid have been studied. The rGO₃-CeO₂ NWs composite exhibited better catalytic performance with slow attenuation and high limiting current density 3.55 and 1.99 times higher than CeO₂ NWs and pure GO. The onset potential of rGO₃-CeO₂ NWs is 0.13 V and 0.05 V positive shift from that of CeO₂ NWs and pure GO, respectively, suggesting that the rGO₃-CeO₂ NWs hybrid has been an excellent stability and activity for ORR. It has been found that CeO₂ NWs served not only as an effective catalyst but also as an “oxygen buffer” to relieve oxygen insufficiency for ORR.

Keywords: CeO₂ nanowires, Reduced graphene oxide, Synergistic effects, Oxygen reduction reaction

Sustainable energy storage and conversion technologies have been extensively developed due to the rapid depletion of fossil fuels and harmful emissions of carbon to the atmosphere¹. Polymer electrolyte membrane fuel cells (PEMFCs) can convert chemical energy into electrical energy with high efficiency of power generation and cleanly emission, which has been the focus in cogeneration systems and vehicle applications^{2,3}. Pt and other precious metal catalysts have been considered as the best electrocatalysts for oxygen reduction reaction (ORR), they still suffer from the sluggish ORR kinetics, susceptibility to time-dependent stability and CO poisoning^{4,5}, which seriously reduce the cathode potential and decrease fuel efficiency. For these problems, highly active and durable electrocatalysts for the ORR have long been the key to the performance of PEMFCs and their commercialization. Over the past few years, much effort had been devoted to the development of different types of non-noble metal catalysts such as metal-based complexes (Fe and Co)⁶⁻⁸, transition

metal oxides (sulfides)⁹⁻¹¹, nitrides^{12,13}, and heteroatom-doped carbon materials^{14,15}.

Recently, transition metal oxides¹⁶⁻¹⁹ such as TiO₂, Fe₃O₄, MnO₂ and Co₃O₄ have been well studied as promising candidates for high-performance cathodes in PEMFCs due to abundant hydroxyl groups on the surfaces of the transition metal oxides, low cost, acid-base resistance property and high stability. CeO₂ serves as one of the most important systems because of the variable valence states of Ce cations and a high oxygen storage capacity. However, poor ionic mobility and low electrical conductivity of transition metal oxides need to be resolved by synthesizing nanomaterials with diverse shapes, porous or interconnected structure and composited with conductive carbon materials. Nowadays, incorporation of transition metal oxides with carbon-based materials such as amorphous carbons²⁰, carbon nanotubes (CNT)²¹, graphene nanosheets²², is an effective strategy to enhance the electrical conductivity and reduce the agglomeration of metal oxides during the electrochemical cycling, favoring

the long-term stability of the fuel cells. It is well known that one-dimensional (1D) nanowires and nanotubes (NTs) have demonstrated excellent performance due to their unique 1D morphologies and high surface area.

Herein, we report design and synthesis of a novel interconnected nano-architecture assembled by graphene nanosheets and CeO_2 NWs. Such a hybrid can be profited from the synergistic effects of each component including (i) The imbedded CeO_2 NWs effectively inhibiting the graphene from restacking and restraining the coiled or folded GO sheets to provide more channels for electron conduction; (ii) Creating oxygen vacancies to generate localized electrons on the surface to induce an intimate contact between GO sheets and CeO_2 NWs, and (iii) Porous structure for fuel transport compared with those of pure GO and CeO_2 NWs.

Materials and Methods

Preparation of rGO- CeO_2 NWs hybrids

CeO_2 NWs were synthesized according to a modified hydrothermal method²³. $\text{CeCl}_3 \cdot 7\text{H}_2\text{O}$ (0.2515 g) and NaCl (0.523 g) were dissolved in water (6 mL) by sonication. Then, 7.5 mL of NaOH solution (12 M) was injected into the suspension. The suspension was stirred and heated at 180 °C for 30 h in a 25 mL Teflon-lined stainless steel autoclave. The products were washed with deionized (DI) water and dried at 50 °C. Finally, the dried products were calcined at 300 °C for 1 h. GO was obtained by a modified Hummers' method²⁴.

A hydrothermal method was employed to synthesize rGO- CeO_2 NWs composites²⁵. About 60 mg GO and CeO_2 NWs mixture in varying ratios was uniformly mixed with a solution of ethanol/water (1:1) by sonication and stirring, until a homogeneous suspension was achieved. The suspension was transferred to a Teflon-lined autoclave (100 mL) and heated at 120 °C for 4 h. The reduction of GO could be achieved using ethanol as a reductant. rGO- CeO_2 NWs nanocomposites were purified by centrifugation, washed with DI water and dried under vacuum at 60 °C for 12 h. The composites at other different graphene to CeO_2 NWs ratios were : 40 mg-20 mg, 45 mg-15 mg and 48 mg-12 mg labeled²⁶ as rGO₂- CeO_2 NWs, rGO₃- CeO_2 NWs and rGO₄- CeO_2 NWs.

Characterization

Structure Characterization

XRD data of the catalysts were collected using a D/max-r B diffractometer (Japan) using a Cu K α

X-ray source operating at 45 kV and 100 mA, scanning at a rate of 8° min⁻¹ with an angular resolution of 0.05° of 2 θ scan. Scanning electron microscopy (SEM) images were taken on a Leo 1530 field-emission scanning electron microscope. X-ray photoelectron spectroscopy (XPS) was used to determine the chemical state of Pt and Ru with a physical electronics PHI model 5700 instrument.

Electrochemical Activity Characterization

All the electro-chemical measurements were conducted using CHI 760E electro-chemical workstation, with a conventional three-electrode setup at 25 °C working electrodes with the catalysts were prepared as follows. A conventional three electrode cell was employed with a platinum wire as the counter electrode, a saturated Hg/HgO electrode as the reference electrode, and a glassy carbon (GC) electrode (diameter = 5 mm) with coated catalysts serving as the working electrode. The catalyst ink was produced by mixing 5 mg of the catalyst under sonication for 30 min in 2.5 mL of ethanol. The suspension (5 μL) was transferred to the surface of the polished glassy carbon electrode and dried in the air at room temperature, then covered with Nafion. The above three electrodes and a 0.1 M KOH solution were used to form a three-electrode system for electrochemical measurements. CV (Cyclic Voltammetry) tests were performed in N₂ and O₂ saturated electrolytes. LSV (linear sweep voltammetry) tests were performed at a rotating rate varying from 500 to 2500 rpm. To check CH₃OH tolerance of the prepared samples, 20000 ppm CH₃OH was added to the electrolyte, and another LSV test was performed at 1600 rpm.

Results and Discussion

SEM images of CeO_2 NWs, GO and rGO₃- CeO_2 NWs hybrid are shown in Fig. 1. It can be seen from Fig. 1a that the fairly uniform CeO_2 NWs was obtained with diameter (20–35 nm) and length (1–3 μm). SEM images of pure GO (Fig. 1b) is exhibiting much clearly visible wrinkles with multilayer and rougher surfaces. As demonstrated in Fig. 1c and Fig. 1d, the rGO₃- CeO_2 NWs hybrid is constructed from uniform 1D CeO_2 NWs and thin-layered graphene nanosheets. The CeO_2 NWs were closely threaded through the thin graphene layers, leading to the formation of an interlaced three-dimensional conductive network. EDS-mapping spectra (Fig. 1e–1h) exhibited a homogeneous dispersion of the catalyst, confirming

the uniform distributions of Ce (in blue), C (in green) and O (in red) along the 1D CeO₂ NWs, suggesting the well dispersed CeO₂ NWs with graphene could restrain the wrinkle of GO.

For the crystal structure of the as-prepared catalysts, as illustrated in Fig. 2, XRD of GO showed the typical

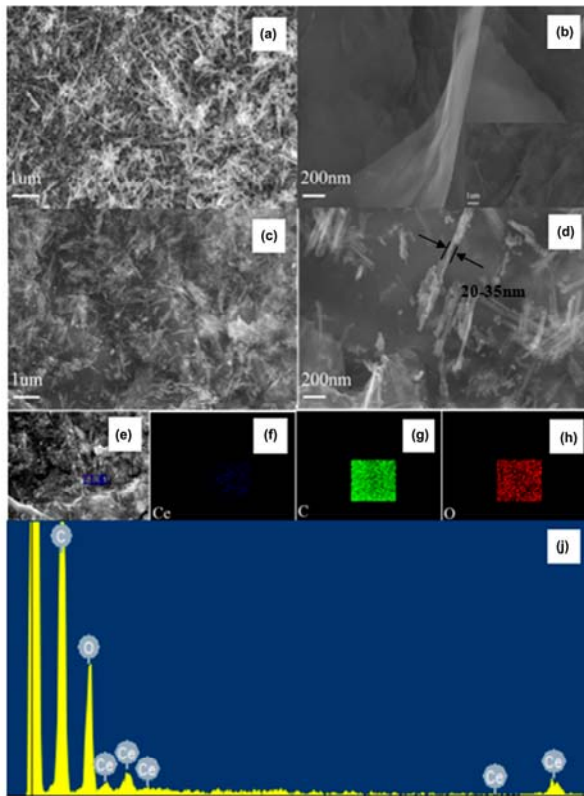


Fig.1 — SEM image of (a) CeO₂ NWs, (b) pure GO and (c-d) GO₃-CeO₂ NWs hybrid structure, (e-h) EDS-mapping spectra, Ce (in blue), C (in green) and O (in red) and (i) EDS analysis of rGO₃-CeO₂ NWs.

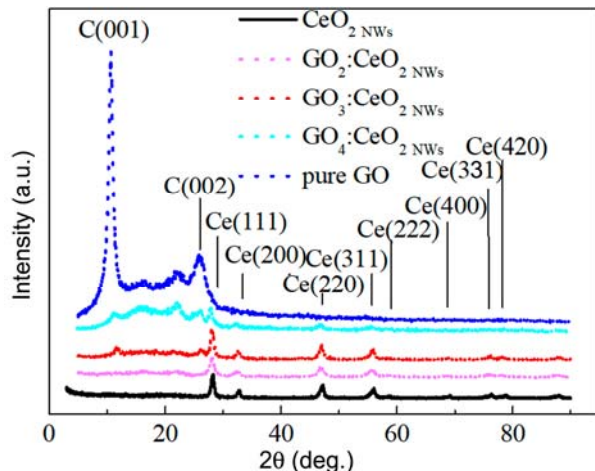


Fig.2 — XRD patterns of CeO₂ NWs, pure GO and rGO₃-CeO₂ NWs hybrid composites with different ratio.

diffraction peak at an angle of 11.3° for the (001) plane due to the formation of the oxygen-containing functional groups on the surface of the GO sheets²⁶. The as-prepared rGO-CeO₂ NWs composites with a different ratio displayed a broad and weak diffraction peak at 24.6°, arising from the (002) reflection of GO sheets, confirming the existence of reduced graphene oxide. However, the diffraction peaks attributing to graphite carbon for the (001) plane could be observed with the increased CeO₂ NWs content in the XRD patterns of rGO-CeO₂ NWs composites, which may be attributed to the low intensity and low mass ratio as well as the formation of threaded CeO₂ NWs on the graphene surface. Meanwhile, the intense peaks at $2\theta = 28.6^\circ, 33.2^\circ, 47.5^\circ, 56.6^\circ, 58.9^\circ, 66.9^\circ, 76.9^\circ$ and 79.1° can be indexed to (111), (200), (220), (311), (222), (400), (331) and (420) reflections of crystalline CeO₂ (JCPDS 81-0792), respectively.

X-ray photo-electron spectroscopy (Fig. 3) illustrated the compositions of rGO₃-CeO₂ NWs composite and the mechanism of the interactions between GO₃ and CeO₂ NWs. The full survey of rGO₃-CeO₂ NWs hybrid displays the signals of Ce 3d, O 1s, and C 1s in the range of 0–1400 eV in Fig. 3a, confirming the successful recombination of GO and CeO₂ NWs. The deconvolution peaks of Ce 3d, O 1s, and C 1s are shown in Fig. 3b, 3c, and 3d, respectively. For Ce 3d peaks (Fig. 3b), four featured peaks locating at 883.7, 889.7, 890.2, and 901.8 eV depict the Ce element chemical states, and fingerprint peak at 917.6 eV is the strong evidence for the presence of Ce⁴⁺, and the peaks located at 886.6 and 904.5 eV are the typical peaks^{27,28} of Ce³⁺. The Ce3d spectrum revealed the coexistence of Ce³⁺ and Ce⁴⁺ species with Ce⁴⁺ being the main valence state in the rGO₃-CeO₂ NWs hybrid. It is known that the change of valence state of CeO₂ from Ce⁴⁺ to Ce³⁺ will introduce oxygen vacancies and unsaturated chemical bond, which activates oxygen in the redox processes, and makes the charge transfer from mobile holes in graphene layers to localized electrons on CeO₂ NWs, thus leading to the great improvement in oxygen reduction on the rGO₃-CeO₂ NWs catalyst²⁹⁻³¹. The C1s spectra (Fig. 3c) displayed the presence of nonoxygenated carbon at 285.3 eV (C=C/C-C), epoxy group at 287.6 eV (C=O), and ester group³² at 289.3 eV (O-C=O). The content of nonoxygenated carbon increased due to a successful reduction of GO in the composite. Spectrum of the O1s (Fig. 3d) was deconvoluted into the carboxylate and ester group (C-OH at 533.7 eV and O-C=O at 531.7 eV), which is

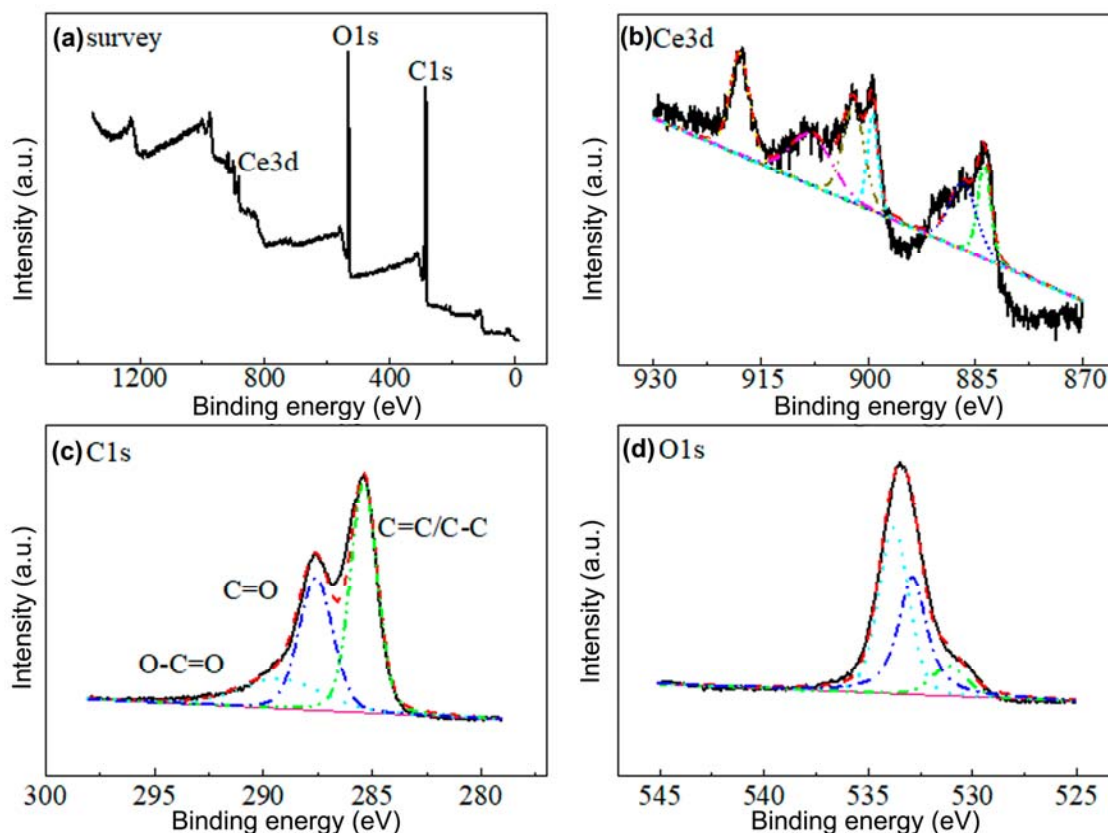


Fig.3 — (a) Survey spectra of catalyst for $\text{rGO}_3\text{-CeO}_2$ NWs hybrid composite, and deconvolution of peaks (b) Ce 3d, (c) C1s, and (d) O 1s spectrum.

in accordance with the above C1s spectra and a new peak locating at 531.0 eV corresponding to the Ce-O bond gives a very strong evidence for the presence of electron transfer^{27, 28, 33} between GO and CeO_2 . The peaks at 531.0 and 531.7 eV belong to the lattice oxygen whereas the one at 533.7 eV corresponds to the chemisorption oxygen³³ such as $-\text{OH}$. The improvement of the redox performance for the catalyst maybe derived from the transformation between oxide species and favored the electron transfer³⁴.

Rotating disk electrode (RDE) technology was used to evaluate the electrocatalytic activity of catalysts. The LSV curves for different samples at a rotating speed of 1600 rpm are shown in Fig. 4a. It can be seen that CeO_2 NWs and pure GO catalysts exhibited a very low ORR electrocatalytic activity. Incorporation of CeO_2 NWs with pure GO and introduction of heterogeneous contact-interface between them resulted in a remarkably increased the diffusion-limited current density and the highest value reached on $\text{rGO}_3\text{-CeO}_2$ NWs at 1600 rpm. In addition, positive shifts at 0.13 V and 0.05 V were observed for onset potential on $\text{rGO}_3\text{-CeO}_2$ NWs (onset potential of

0.91 V vs. RHE) compared to CeO_2 NWs (onset potential of 0.78 V vs. RHE) and pure GO (onset potential of 0.86 V vs. RHE) catalysts, respectively, indicating enhanced ORR performance. $\text{rGO}_3\text{-CeO}_2$ NWs hybrid contained more active sites and more easily accessible to adsorb O_2 , making a great contribution to catalytic activities. The Tafel slopes in Fig. 4b were obtained from the linear plots of LSV to comprehensively understand the difference of ORR kinetics among rGO-CeO_2 NWs hybrids, CeO_2 NWs and pure GO. A slope of 56.0 mV dec^{-1} can be observed for $\text{rGO}_3\text{-CeO}_2$ NWs, which is much lower than that of CeO_2 NWs ($98.34 \text{ mV dec}^{-1}$), pure GO ($83.35 \text{ mV dec}^{-1}$) and Pt/C (79.2 mV dec^{-1})³⁵, suggesting a much better kinetic behavior for ORR. Also, the electron-transfer resistance of $\text{rGO}_3\text{-CeO}_2$ NWs hybrid showed the smallest semicircle according to the electrochemical impedance spectra (EIS) presented in Fig. 4c, indicating the hybrid could efficiently enhance the conductivity and improve the catalytic activity for ORR due to the synergetic chemical coupling between GO and CeO_2 NWs. Furthermore, the durability of the rGO-CeO_2 NWs hybrid, CeO_2 NWs and

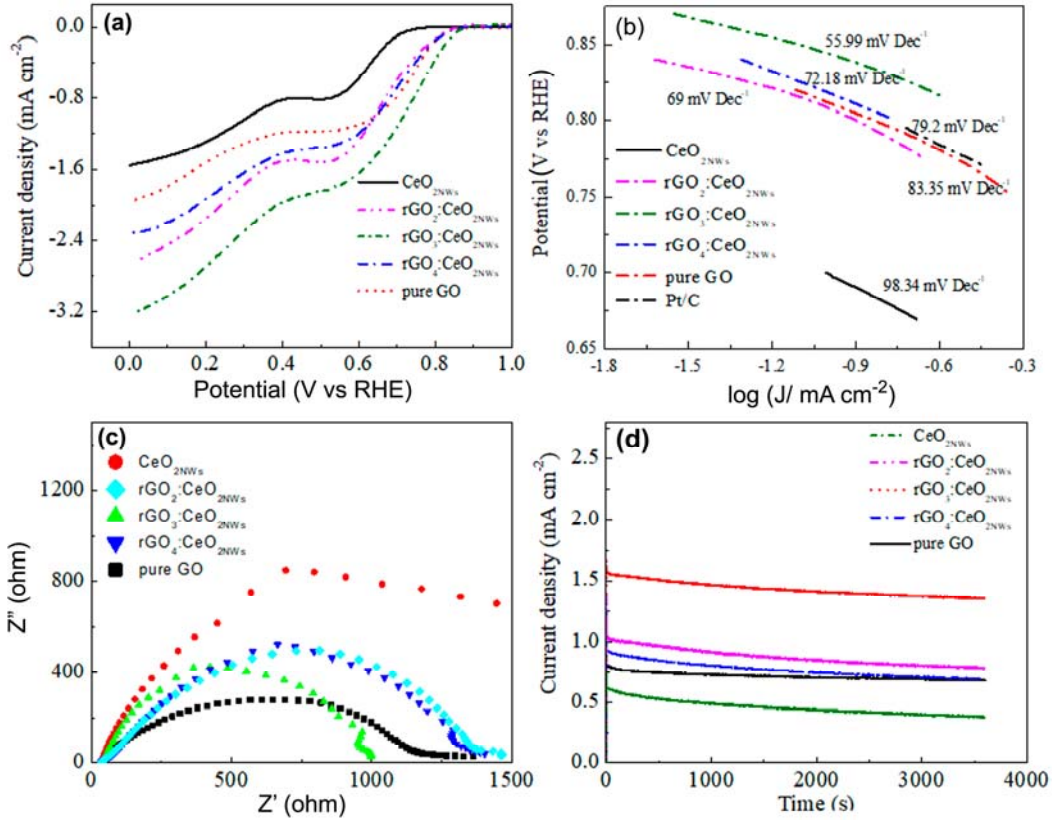


Fig. 4 — (a) LSV curves of rGO-CeO₂ NWS hybrid composites, CeO₂ NWS and pure GO; (b) Tafel plot of kinetic current for different catalysts; (c) Nyquist plots obtained from EIS of different catalysts; (d) *i-t* curves for the different sample at 0.625 V. Supporting electrolyte: 0.1 M KOH Scan rate: 10 mV s⁻¹.

pure GO were evaluated by *i-t* curves (Fig. 4d). It was observed that the response of the rGO₃-CeO₂ NWS hybrid exhibited a very slow attenuation with a high current retention after 3600 s, which is 3.55 and 1.99 times higher than CeO₂ NWS and pure GO, suggesting that the rGO₃-CeO₂ NWS hybrid had an excellent stability. CeO₂ NWS can serve not only as an effective catalyst but also as an “oxygen buffer” to relieve oxygen insufficiency for ORR.

We further studied the ORR catalytic activities of rGO₃-CeO₂ NWS hybrid in N₂- and O₂-saturated 0.1 M aqueous KOH electrolyte solutions by CV curves at a scan rate of 50 mV s⁻¹ (Fig. 5a). In N₂-saturated solution, the CV curve presented no obvious reduction peak between 0 and 1.2 V. In contrast, when O₂ was saturated in the electrolyte, the curve presented a clear increase in current density at around 0.92 V, suggesting the remarkable ORR performance. In the meantime, RDE measurements also exhibited that the diffusion-limited current density on rGO₃-CeO₂ NWS hybrid increased with increasing rotation rate from 500 to 2500 rpm (Fig. 5b). The onset ORR potential is kept almost constant at around 0.91 V

within the rotation rate. The corresponding Koutecky-Levich (K-L) plots on the rGO₃-CeO₂ NWS hybrid (Fig. 5c) demonstrated the inverse current density ($-J$)⁻¹ as a function of the inverse of the square root of the rotation speed ($\omega^{-1/2}$) at several potentials. The transferred electron numbers per O₂ and kinetic current density in the ORR were determined by the Koutecky-Levich equation^{36,37}.

$$\frac{1}{J} = \frac{1}{J_k} + \frac{1}{B\omega^{1/2}} \quad \dots (1)$$

$$B = 0.2 n F C_0 D_0^{2/3} \gamma^{-1/6} \quad \dots (2)$$

where J is the measured current density and J_k is the kinetic current density. n represents the overall number of electrons gained per O₂, F is the Faraday constant (96485 C mol⁻¹), C_0 is the bulk concentration of O₂ (1.1×10⁻³ mol L⁻³), D_0 is the diffusion coefficient of O₂ in 0.1 M KOH (1.9×10⁻⁵ cm² s⁻¹) and γ is the kinetic viscosity of the electrolyte (0.01 cm² s⁻¹). The constant 0.2 was adopted when the rotation rate was expressed in rpm. Remarkable enough, the electron transfer number n for ORR at the

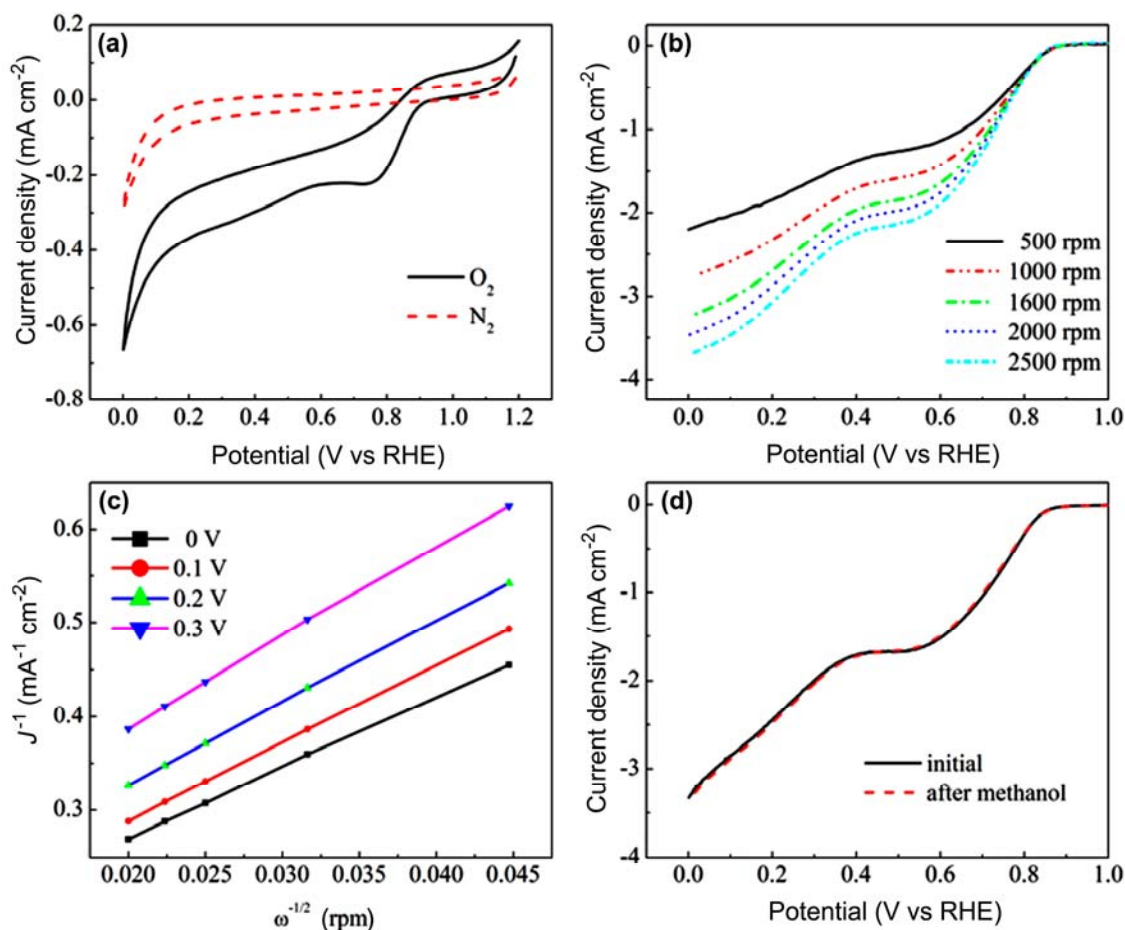


Fig.5 — (a) CV curves of ORR on the $rGO_3-CeO_2_{NWS}$ hybrid composite electrodes in N_2 - and O_2 -saturated 0.1 M KOH at a scan rate of 10 mV s^{-1} , (b) LSV curves at various rotating ration at a scan rate of 10 mV s^{-1} , (c) Koutecky-Levich plots at 0, 0.1, 0.2 and 0.3 V, and, (d) $rGO_3-CeO_2_{NWS}$ hybrid composite in O_2 -saturated 0.1 M KOH solution with and without CH_3OH .

$rGO_3-CeO_2_{NWS}$ hybrid catalyst was calculated as 2.92–3.75 from 0 to 0.3 V (vs. RHE), which revealed that the electrocatalytic process of $rGO_3-CeO_2_{NWS}$ hybrid is almost a four-electron pathway for ORR and favorable for most cathodic reaction for a fuel cell. It is known that the methanol tolerance is an important factor for the catalyst especially in a direct methanol fuel cell (DMFC) since the methanol crossover effects lead to a seriously reduced performance for fuel cells. Addition of 1 M methanol to the O_2 -saturated electrolyte does not because a significant decrease in onset potential for $rGO_3-CeO_2_{NWS}$ hybrid as shown in Fig. 5d, indicating it is free of poisoning effects from methanol and an excellent non-precious catalyst towards ORR.

Conclusions

We have developed a facile hydrothermal approach to fabricate $rGO_x-CeO_2_{NWS}$ hybrids as an ORR electrocatalytic catalyst. The ORR activity of rGO_3-

CeO_2_{NWS} significantly favored a four-electron pathway in the ORR due to the synergistic effect between GO and CeO_2_{NWS} . The $rGO_3-CeO_2_{NWS}$ hybrids showed a very slow attenuation with a high current retention and remarkable increased the diffusion-limited current density at 1600 rpm compared to CeO_2_{NWS} and pure GO, as well as its free of poisoning effects from methanol towards ORR. The increased conductivities and catalytic activity were ascribed to the synergetic chemical coupling between GO and CeO_2_{NWS} , and CeO_2_{NWS} served not only as an effective catalyst but also as an “oxygen buffer” to relieve oxygen insufficiency for ORR. The strategy of using GO and CeO_2_{NWS} hybrid as a catalyst with high performance and low cost provides a potential candidate for fuel cells.

Acknowledgement

The present work is financially supported by the National Natural Science Foundation of China (Grant

No. 21206124, No. 21506159, No. 51478314 and No. 51638011), National Key Research and Development Plan (2016YFC0400503, 2016YFC0400506), Natural Science Foundation of Tianjin (No.12JCZDJC28400 and No.12JCQNJC-7208600), and the Science and Technology Plans of Tianjin (No. 15PTSJYC00230).

References

- 1 Luo J, Im J H, Mayer M T, Schreier M, Nazeeruddin M K, Park N G, Tilley S D, Fan H J & Graetzel M, *Sci*, 345 (2014) 1593.
- 2 Springer T E, Zawodzinski T A & Gottesfeld S, *J Electrochem Soc*, 138 (1991) 2334.
- 3 Steele B C H & Heinzl A, *Nature*, 414 (2001) 345.
- 4 Zhu C Z & Dong S J, *Nanoscale*, 5 (2013) 1753.
- 5 Bai X, Shi Y, Guo J, Gao L, Wang K, Du Y & Ma T, *J Power Sources*, 306 (2016) 85.
- 6 Lin L, Zhu Q & Xu A W, *J Am Chem Soc*, 136 (2014) 11027.
- 7 Wen Z, Ci S, Zhang F, Feng X, Cui S, Mao S, Luo S & He Z, *Adv Mater*, 24 (2012) 1399.
- 8 Mamlouk M, Kuma S M S & Gouerec P, *J Power Sources*, 196 (2011) 7594.
- 9 Cheng F, Su Y, Liang J, Tao Z & Chen J, *Chem Mater*, 22 (2010) 898.
- 10 Wu Z S, Yang S, Sun Y, Parvez K, Feng X & Mullen K, *J Am Chem Soc*, 134 (2012) 9082.
- 11 Wang H, Liang Y, Li Y & Dai H, *Angew Chem Int Ed Engl*, 50 (2011) 10969.
- 12 Dong Y Z, Wu Y M, Liu M J & Li J H, *Chemsuschem*, 6 (2013) 2016.
- 13 Liu M, Dong Y, Wu Y, Feng H & Li J, *Chemistry*, 19 (2013) 14781.
- 14 Gong Y, Fei H, Zou X, Zhou W, Yang S, Ye G, Liu Z, Peng Z, Lou J, Vajtai R, Yakobson B I, Tour J M & Ajayan P M, *Chem Mater*, 27 (2015) 1181.
- 15 Wohlgemuth S A, White R J, Willinger M G, Titirici M M & Antonietti M, *Green Chem*, 14 (2012) 1515.
- 16 Guo L M, Liang K, Marcus K, Li Z, Zhou L, Mani P D, Chen H, Shen C, Dong Y J, Zhai L, Coffey K R, Orlovskaya N, Sohn Y H & Yang Y, *ACS Appl Mater Inter*, 8 (2016) 34970.
- 17 Almeida I, Mendo S G, Carvalho M D, Correia J P & Viana A S, *Electrochimica Acta*, 188 (2016) 1.
- 18 Yu Q, Xu J, Wu C, Zhang J & Guan L, *ACS Appl Mater Inter*, 8 (2016) 35264.
- 19 Liu K, Huang X, Wang H, Li F, Tang Y, Li J & Shao M, *ACS Appl Mater Inter*, 8 (2016) 34422.
- 20 Zhang C, Wang B, Shen X, Liu J, Kong X, Chuang S S C, Yang D, Dong A & Peng Z, *Nano Energy*, 30 (2016) 503.
- 21 Zhao S & Rasimick B, Mustain W & Xu H, *Appl Catal B: Environ*, 203 (2017) 138.
- 22 Kong D, Yuan W, Li C, Song J, Xie A & Shen Y, *Appl Surf Sci*, 393 (2017) 144.
- 23 Ke J, Xiao J W, Zhu W, Liu H, Si R, Zhang Y W & Yan C H, *J Am Chem Soc*, 135 (2013) 15191.
- 24 Hummers Jr W H & Offeman R E, *J Am Chem Soc*, 80 (1958) 1339.
- 25 Yu S, Liu Q, Yang W, Han K, Wang Z & Zhu H, *Electrochim Acta*, 94 (2013) 245.
- 26 Park S, Lee K S, Bozoklu G, Cai W, Nguyen S T & Ruoff R S, *ACS nano*, 2 (2008) 572.
- 27 Shan W P, Liu F D, He H, Shi X Y & Zhang C B, *Appl Catal B-Environ*, 115 (2012) 100.
- 28 Fang J, Bi X Z, Si D J, Jiang Z Q & Huang W X, *Appl Surf Sci*, 253 (2007) 8952.
- 29 Wohlgemuth S A, White R J, Willinger M G, Titirici M M & Antonietti M, *Green Chem*, 14 (2012) 1515.
- 30 Zhu W J, Zhang J, Gong X Q & Lu G, *Cataly Today*, 165 (2011) 19.
- 31 Joung D, Singh V, Park S, Schulte A, Seal S & Khondaker S I, *J Phys Chem C*, 115 (2011) 24494.
- 32 Cong H P, Ren X C, Wang P & Yu S H, *ACS Nano*, 6 (2012) 2693.
- 33 Gao F Y, Tang X L, Yi H H, Li J Y, Zhao S Z, Wang J G, Chu C & Li C L, *Chem Eng J*, 317 (2017) 20.
- 34 Lu X, Song C, Chang C C, Teng Y, Tong Z & Tang X, *Ind Eng Chem Res*, 53 (2014) 11601.
- 35 Jin H, Huang H, He Y, Feng X, Wang S, Dai L & Wang J, *J Am Chem Soc*, 137 (2015) 7588.
- 36 Liang Y, Wang H, Zhou J, Li Y, Wang J, Regier T & Dai H, *J Am Chem Soc*, 134 (2012) 3517.
- 37 Xiong W, Du F, Liu Y, Jr. A P, Supp M, Ramakrishnan T S, Dai L & Jiang L, *J Am Chem Soc*, 132 (2010) 15839.